



Ionic liquid-induced strategy for porous perovskite-like PbBiO_2Br photocatalysts with enhanced photocatalytic activity and mechanism insight

Bin Wang^a, Jun Di^a, Pengfei Zhang^b, Jiexiang Xia^{a,b,**}, Sheng Dai^{b,*}, Huaming Li^{a,*}

^a School of Chemistry and Chemical Engineering, Institute for Energy Research, Jiangsu University, 301 Xuefu Road, Zhenjiang 212013, PR China

^b Chemical Sciences Division, Oak Ridge National Laboratory, Oak Ridge, USA



ARTICLE INFO

Article history:

Received 2 October 2016

Received in revised form

15 December 2016

Accepted 19 December 2016

Available online 21 December 2016

Keywords:

PbBiO_2Br microspheres

Visible light irradiation

Photocatalysts

Ionic liquid

ABSTRACT

A novel perovskite-like PbBiO_2Br uniform porous microspheres photocatalyst was successfully prepared via ethanol glycol (EG)-assisted solvothermal method in the presence of reactable ionic liquid 1-hexadecyl-3-methylimidazolium bromide ($[\text{C}_{16}\text{mim}]^+\text{Br}^-$) and polyvinyl-pyrrolidone (PVP) system. During the synthetic process, the ionic liquid-PVP complex system acts as the solvent, reactant and template simultaneously, and demonstrates excellent control capability for PbBiO_2Br porous microstructure. The photocatalytic activity of the PbBiO_2Br materials was evaluated by colorless antibiotic agent ciprofloxacin (CIP), endocrine disrupter bisphenol A (BPA), and colored rhodamine (RhB), methylene blue (MB) as target pollutants under visible light irradiation. After several characterizations, the influencing factor of the promotional photocatalytic activity for PbBiO_2Br photocatalysts was discussed in detail. Through the ESR and trapping experiment verification, the superoxide radical ($\text{O}_2^{\cdot-}$) and hole (h^+) were the main active species for the photocatalysis process.

© 2016 Elsevier B.V. All rights reserved.

1. Introduction

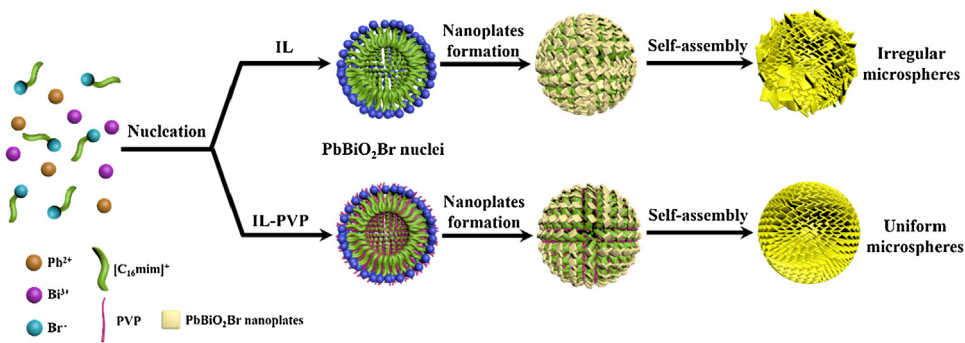
The semiconductor photocatalytic materials because of their wide applications have been attracted massive research interest in solar energy conversion and environmental decontamination during the several years [1–3]. Meanwhile, perovskite (ABX_3) has paid close attention to play important roles in photocatalysis and photovoltaics. These materials can be used as photocatalysts for photo-degradation of organic dyes in wastewater, light absorbers solar cells for electricity generation, and water splitting reaction for hydrogen production [4–6]. In recent years, various perovskite photocatalysts have been reported subsequently with excellent photocatalytic activity, such as $\text{Sr}_2\text{M}_2\text{O}_7$ ($\text{M}=\text{Nb}$ and Ta) [7], NaTaO_3 [8], $\text{La}_2\text{Ti}_2\text{O}_7$ [9], MBiO_2Cl ($\text{M}=\text{Sr}, \text{Ba}$) [10], and so on.

As one of a new class promising photocatalyst, PbBiO_2Br began to be widely attention owing to controllable morphology, suitable band gaps, high stability, and good visible-light photocatalytic activity [11,12]. Nowadays, several methods could synthesize the PbBiO_2Br catalyst, such as solid-state reaction [13], solvothermal method [14] etc. Huang et al. synthesized layered PbBiO_2Br by a solid state reaction at different temperature (700 °C–900 °C), which could remove RhB under UV and visible light irradiation [13]. Yang's group prepared ultrathin PbBiO_2Br nanosheets via a solvothermal method (180 °C) using CTAB as the bromine source and regulating pH by ammonia water, and the nanosheets exhibited photocatalytic activity towards the degradation of methyl orange (MO) dye under visible light [14]. Cherevatskaya and co-workers explored stirring for 72 h at 80 °C in a round bottom flask with stopper realized the synthesis of PbBiO_2Br nanosemiconductor [15]. Those PbBiO_2Br materials all revealed excellent photocatalytic activity for the degradation of dyes. Nevertheless, previous research results assume that the PbBiO_2Br catalysts usually exhibit uncontrolled crystallinity and morphology even minor specific surface area by the solid state chemistry with large energy consumption in the high reaction temperature. Moreover, all of the previous research explored the degradation of color dye briefly, while the colorless pollutants have not be considered, such as antibiotics and

* Corresponding authors.

** Corresponding author at: School of Chemistry and Chemical Engineering, Institute for Energy Research, Jiangsu University, 301 Xuefu Road, Zhenjiang 212013, PR China.

E-mail addresses: xjx@ujs.edu.cn (J. Xia), dais@ornl.gov (S. Dai), [\(H. Li\).](mailto:lhm@ujs.edu.cn)



Scheme 1. Schematic representation of the synthesis process of PbBiO_2Br samples.

endocrine disrupters. As is known to all, the porous or hollow microscopic structure with excellent adsorption capability could promote photocatalytic activity under light irradiation. Therefore, the exploration of PbBiO_2Br porous micro/nanomaterials with uniform morphology, large specific surface area and high stability remains to be explored to meet the ever-increasing demand.

Currently, ionic liquids (ILs) have been concerned for the preparation of micro/nanomaterials because of low viscosity, large thermal capacity, stable in the moist air and efficient dissolving capacity [16,17]. As the novel “green solvents” and “designability solution”, ILs have been applied in the synthesis of functional materials with different size and morphology such as $\text{Bi}_4\text{O}_5\text{Br}_2$ ultrathin nanosheets [18], $\alpha\text{-Fe}_2\text{O}_3$ cubes [19], BiOI hollow microspheres [20], CuO peachstone-like architectures [21], Au nanosheets [22] etc. In these systems, ionic liquids acted as solvents, templates, and reactants for the various catalysts preparation. Meanwhile, numerous explorations revealed that ionic liquids could combine with surfactants to form multiple micelles in the solutions, which could improve the control ability of the system [23,24]. Kaper et al. have reported the preparation of WO_3 films by the presence of the ionic liquids 1-hexadecyl-3-methyl imidazolium chloride and bromide and surfactants cetyltrimethylammonium chloride and bromide [25]. The new plasmonic photocatalyst three-dimensional hierarchical $\text{Ag}/\text{AgI}/\text{BiOI}$ microspheres have been successfully synthesized via a reactive ionic liquid 1-butyl-3-methylimidazolium iodine and surfactant polyvinylpyrrolidone system [26]. BiOCl and BiOBr uniform porous structures have been prepared in the presence of reactable ionic liquid and surfactant PVP composite system in our previous works [27,28]. The previous studies demonstrated that ionic liquid-surfactant(IL-S) complex system was conducive to the structural regulation of the functional materials. Therefore, the potential of IL-S complex system in the controlled synthesis of PbBiO_2Br hierarchical porous-structure materials is meaningful and still needs to be fully explored.

In this work, the PbBiO_2Br porous microspheres have been fabricated through EG-assisted solvothermal method process in the presence of IL-S complex system. **Scheme 1** illustrates the synthetic process of PbBiO_2Br materials, which is detailed in the experimental section. During the reactive process, ionic liquid and IL-S system have been designed for the control preparation of PbBiO_2Br materials, respectively. The as-prepared PbBiO_2Br materials exhibited admirable photocatalytic activity, which could not only degrade the artificial dyes rhodamine B (RhB) and methylene blue (MB) but also remove the broad-spectrum antibacterial agent ciprofloxacin (CIP) and the endocrine disrupter bisphenol A (BPA) under visible light irradiation. In addition, the relationship between the structure and the photocatalytic performance of the innovative PbBiO_2Br materials, the active species, and photocatalytic mechanism in the process of photocatalytic reaction have been explored in detail.

2. Experimental

2.1. Preparation of photocatalysts

All chemicals were analytical grade and used without further purification. In a typical synthesis of PbBiO_2Br materials, 1 mmol $\text{Bi}(\text{NO}_3)_3 \cdot 5\text{H}_2\text{O}$ and 1 mmol $\text{Pb}(\text{NO}_3)_2$ were dissolved into 20 mL ethylene glycol containing a certain amount of PVP and 1 mmol ionic liquid $[\text{C}_{16}\text{mim}]^+\text{Br}^-$ solution. The mixture was further stirred for 30 min at room temperature, and then added into 25 mL Teflon-lined autoclave next heated at 140 °C for 24 h. After the obtained samples cooled down to room temperature, subsequently the catalysts were centrifuged and washed with distilled water and ethanol for several times. Then the catalysts were dried under vacuum at 50 °C for 12 h. The added contents of PVP in the PbBiO_2Br photocatalysts were 0, 0.05, 0.10, 0.15, and 0.20 g, which were marked $\text{PbBiO}_2\text{Br-0}$, $\text{PbBiO}_2\text{Br-0.05}$, $\text{PbBiO}_2\text{Br-0.10}$, $\text{PbBiO}_2\text{Br-0.15}$, and $\text{PbBiO}_2\text{Br-0.20}$, respectively.

2.2. Characterization of photocatalysts

The crystalline structure of the materials was analyzed by the powder X-ray diffraction (XRD) pattern on a Shimadzu XRD-6000X-ray diffractometer with monochromatized $\text{Cu-K}\alpha$ radiation ($\lambda = 0.15418 \text{ nm}$). The elements on the surface of the photocatalysts was determined by the X-ray photoelectron spectroscopy (XPS) measured on a PHI5300 with a monochromatic $\text{Mg K}\alpha$ source. The microstructure of the microspheres verified by field emission scanning electron microscopy (SEM) with an energy-dispersive X-ray spectroscope (EDS) and transmission electron microscopy (TEM). The UV-vis spectra was detected by UV-vis spectrometer on an UV-2450 spectrophotometer (Shimadzu Corporation, Japan) with BaSO_4 powder as the reference. The specific surface area and particle size of the materials were obtained via Brunauer-Emmett-Teller (BET) method based on the N_2 adsorption-desorption isotherms. Electron spin resonance (ESR) spectra were acquired on a Bruker model ESR JES-FA200 spectrometer. The photocurrent and the electrochemical impedance spectroscopy (EIS) results were recorded with a CHI 660B electrochemical analyzer in a constructed three electrode system, in which a platinum wire was used as a counter electrode, a $\text{Ag}/\text{AgCl}/\text{sat. KCl}$ acted as reference electrode, the thin film of the as-prepared PbBiO_2Br materials on ITO was used as the working electrode. A 500 W Xe arc lamp served as a light source. The electrolyte of phosphate buffer solution (PBS, 0.1 M, pH 7.0) was used to photocurrent detection, and the EIS was performed in a 0.1 M KCl solution containing 5 mM $\text{Fe}(\text{CN})_6^{3-}/\text{Fe}(\text{CN})_6^{4-}$.

The concentration change of BPA over time was analyzed by high performance liquid chromatography (HPLC) with two Varian ProStar210 pumps, an Agilent TC-C (18) column, and a Varian ProStar325 UV-vis Detector at 230 nm. The mobile phase was a

solution of methanol and H₂O in the ratio 75: 25 (v/v) at 1 mL/min, and 20 µL of the sample solution was injected.

2.3. Photocatalytic activity

The photocatalytic activity of the PbBiO₂Br powers was assessed by the photocatalytic oxidation degradation of CIP, BPA, RhB, and MB under visible light irradiation. All of the concentration of target pollutants was 10 mg/L. During the experiments process, a 300 W Xe arc lamp was used as light source with a UV cutoff filter (400 nm) to provide the visible light and a 580 nm cutoff filter to provide the near-infrared light. A circulating water system (30 °C) prevent the thermal catalytic effects. An air pump was executed to supply sufficient oxygen, and all the while, the solution and photocatalysts was mixed completely by intensive stirring during the photoreactions. In these catalysis experiments, 20 mg PbBiO₂Br catalyst was dispersed into 100 mL of the MB solutions, 50 mg PbBiO₂Br material was dispersed into 100 mL of the BPA solutions, 30 mg PbBiO₂Br power was dispersed into 100 mL of the CIP and RhB solutions, respectively. Photocatalyst and target pollutant established adsorption-desorption equilibrium by magnetically stirred 30 min in the dark ahead of light irradiation. At set intervals, the suspension was withdrawn detection timely, of which the remnant amount of BPA was analyzed by HPLC, and the concentration of RhB, MB, and CIP determined using a UV-vis spectrophotometer at 553 nm, 664 nm, and 276 nm, respectively.

3. Results and discussion

3.1. Structure and morphology characterization of PbBiO₂Br photocatalysts

Using powder XRD measurements could examine the phase and composition of the as-prepared products effectively. The typical XRD patterns of the as-prepared PbBiO₂Br samples obtained through [C₁₆mim]Br ionic liquid and different PVP content were shown in Fig. 1a. The as-prepared samples displayed the diffraction peaks of (101), (103), (110), (006), (200), (211), (116), (213), (206), (220), and (301) planes at $\theta = 23.4^\circ, 30.6^\circ, 31.7^\circ, 42.3^\circ, 45.4^\circ, 51.7^\circ, 53.8^\circ, 55.8^\circ, 63.8^\circ, 66.2^\circ$, and 75.3° , which can be indexed to tetragonal phase of PbBiO₂Br (JCPDS card no. 38-1008). Interestingly, the intensity ratio of the (103) peak to the (110) peak in the as-prepared PbBiO₂Br-0 materials synthesized without PVP was obviously larger than that of the PbBiO₂Br materials synthesized with different content of PVP and the data of the PbBiO₂Br JCPDS card. The important result implied that the PbBiO₂Br materials syn-

thesized with IL-S complex system had special anisotropic growth along the (110) facet, and the PbBiO₂Br materials synthesized without PVP had a higher percentage of (103) facets. No characteristic peaks of the other impurities were observed, which demonstrated that the products were high purity and single phase. The schematic representation of the PbBiO₂Br crystal structure could be seen in Fig. 1b.

The chemical states and the surface element composition of the as-prepared PbBiO₂Br-0 and PbBiO₂Br-0.10 materials were studied by XPS (Fig. 2). The binding energies results were corrected for specimen charging by referencing the C 1s line to 284.6 eV in the XPS analysis. As is shown in Fig. 2a, the survey scan XPS spectrum displayed Pb, Bi, O, and Br peaks of PbBiO₂Br-0 and PbBiO₂Br-0.10 materials, which were consistent with the chemical composition of the samples, when the materials were compounded by using different content of PVP. In the high-resolution Pb 4f spectrum of PbBiO₂Br-0 and PbBiO₂Br-0.10 samples are centered at 138.3 and 143.1 eV (Fig. 2b), which corresponding to Pb²⁺ in the PbBiO₂Br materials [29]. The Bi 4f XPS spectra of PbBiO₂Br-0 and PbBiO₂Br-0.10 crystals are shown in Fig. 2c. The binding energies of Bi 4f_{7/2} and Bi 4f_{5/2} are 159.1 eV and 164.5 eV in the oxide form of PbBiO₂Br [30], respectively, which can be attributed to the Bi atoms existing in a 3+ oxidation state. The O 1s peaks are associated with binding energy of 529.9 eV (Fig. 2d) [31], which can be assigned to the O in PbBiO₂Br materials. Fig. 2e shows high-resolution Br 3d XPS spectra of the sample, in which the two typical peaks located at binding energies of 68.5 eV and 69.5 eV, which is characteristic of Br⁻ in the as-prepared PbBiO₂Br samples [18]. Meanwhile, XRD and XPS results confirmed that the PVP and reactable ionic liquid were removed from the surface of PbBiO₂Br crystal, and the as-samples were pure PbBiO₂Br.

The morphology and microstructure of the as-prepared PbBiO₂Br materials were characterized by SEM and TEM analysis. Fig. S1a is the SEM images of the PbBiO₂Br-0 microspheres synthesized with ionic liquid [C₁₆mim]Br only at 140 °C for 24 h. As can be shown from the SEM image, the average diameter of the PbBiO₂Br-0 was inhomogeneous with some half-baked microspheres and the samples consisted of numerous PbBiO₂Br nanosheets. However, the nanosheets of the PbBiO₂Br-0 materials were short and even anomalous. Interestingly, as shown from the SEM images (Fig. 3a and b), the average diameter of the PbBiO₂Br-0.10 microsphere structures was about 3 µm, which showed more uniform compared to the existing literatures. In addition, it was found that the thickness and size of the smooth PbBiO₂Br-0.10 nanosheets were nearly 20–30 nm and 200–250 nm, respectively. (Fig. 3b inset). The microstructure of the PbBiO₂Br-0.10 materials was further inves-

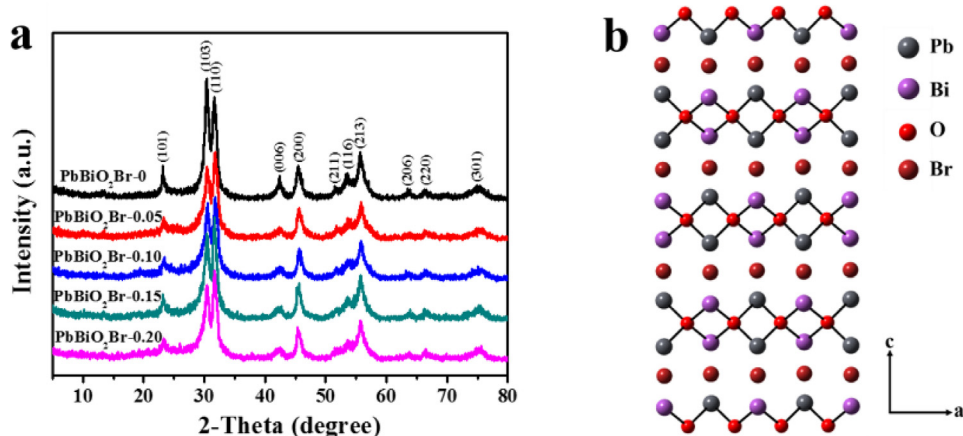


Fig 1. (a) The XRD patterns of the as-prepared PbBiO₂Br materials obtained by using different content of PVP; (b) The crystal structure of PbBiO₂Br.

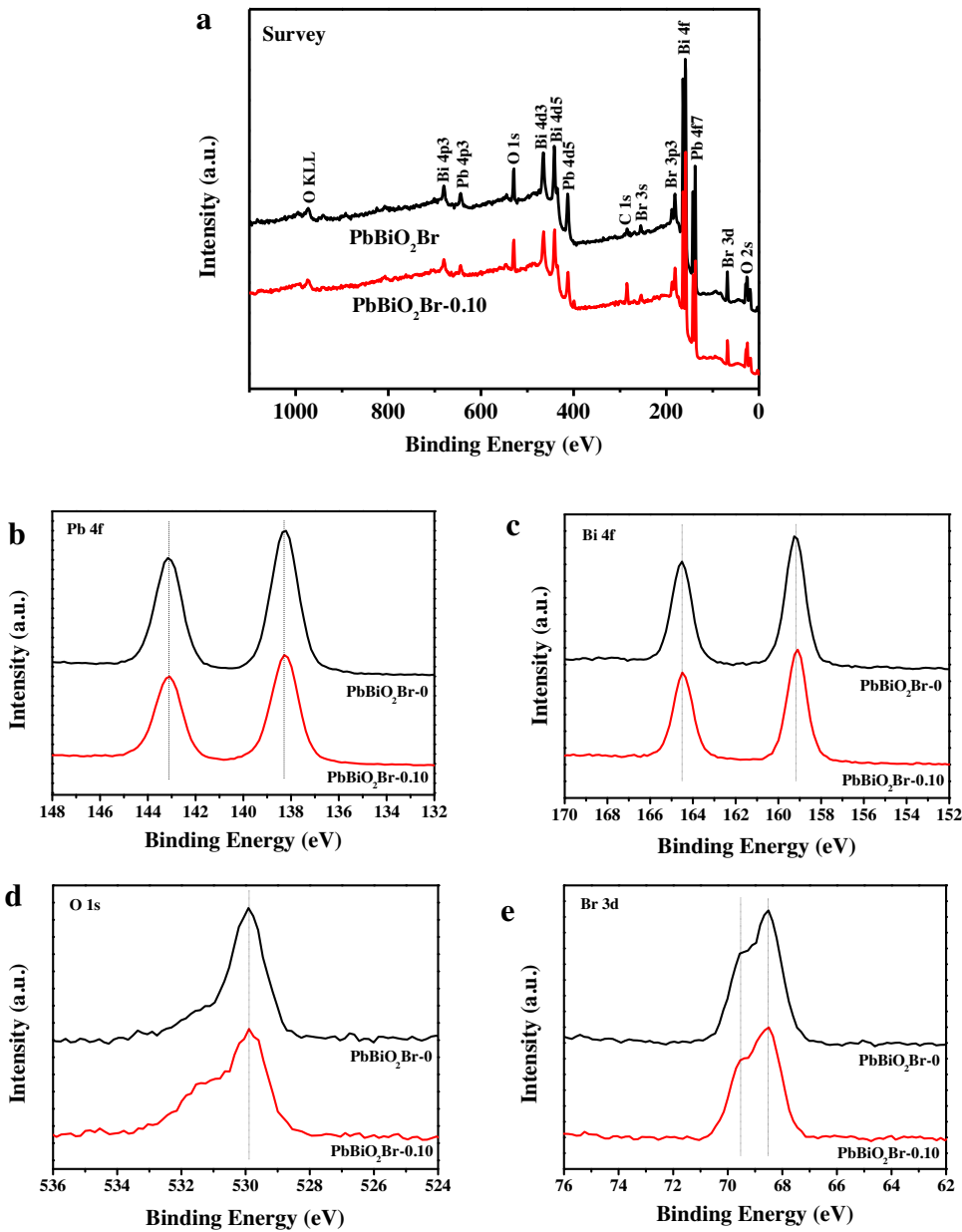


Fig. 2. XPS spectra of the as-prepared PbBiO₂Br-0 and PbBiO₂Br-0.10 samples: (a) survey of the sample; (b) Pb 4f; (c) Bi 4f; (d) O 1s; (e) Br 3d.

tigated by TEM, as is shown in Fig. 3c and d. The TEM images showed the PbBiO₂Br-0.10 microspheres with the solid interior was assembled by nanosheets. The nearly transparent nature of these nanosheets implies the thinner thickness.

The synthesis of PbBiO₂Br materials was obtained by using different content of PVP. It can be seen that the average diameter of the PbBiO₂Br was inhomogeneous, when the additive amount of PVP was 0.05 g (Fig. S1b). However, the nanosheets of the PbBiO₂Br-0.05 microsphere became smoother than the PbBiO₂Br-0 materials. To perform experiments with different additive content of PVP, confirmed that the PbBiO₂Br-0.15 (Fig. S1c) and PbBiO₂Br-0.20 (Fig. S1d) microsphere structures were constituted by the twisty nanosheets and even destroyed by the excessive PVP. According to the control variate method, the result illuminated that the moderate PVP and the ionic liquid [C₁₆mim]Br play an important role in the preparation process of the PbBiO₂Br microsphere materials.

The chemical composition of the PbBiO₂Br-0 and PbBiO₂Br-0.10 microspheres was further confirmed by EDS analysis. The

EDS element mapping clearly showed the elements Pb, Bi, O and Br evenly distributed in PbBiO₂Br-0.10 materials (Fig. S2). These results further proved that the PbBiO₂Br materials have been prepared successfully, which were consistent with the results of the XRD and XPS analyses.

As is shown in Figs. Fig. 4 and S3, the nitrogen adsorption and desorption isotherms were carried out, which could characterize the specific surface area and porosity of the PbBiO₂Br materials. All of the PbBiO₂Br materials obtained by using different content of PVP resembled type IV isotherms, which indicated the products had mesoporous structure [32]. In this system, the specific surface area of the PbBiO₂Br-0 material was 11.76 m² g⁻¹. When the IL-S complex system was introduced into the formation process of PbBiO₂Br materials, the BET specific surface area of them was larger than PbBiO₂Br-0 sample and calculated to be 22.40, 57.75, 21.11 and 19.90 m² g⁻¹ for PbBiO₂Br-0.05, PbBiO₂Br-0.10, PbBiO₂Br-0.15, and PbBiO₂Br-0.20, respectively. Obviously, PbBiO₂Br-0.10 microspheres exhibited the maximum specific sur-

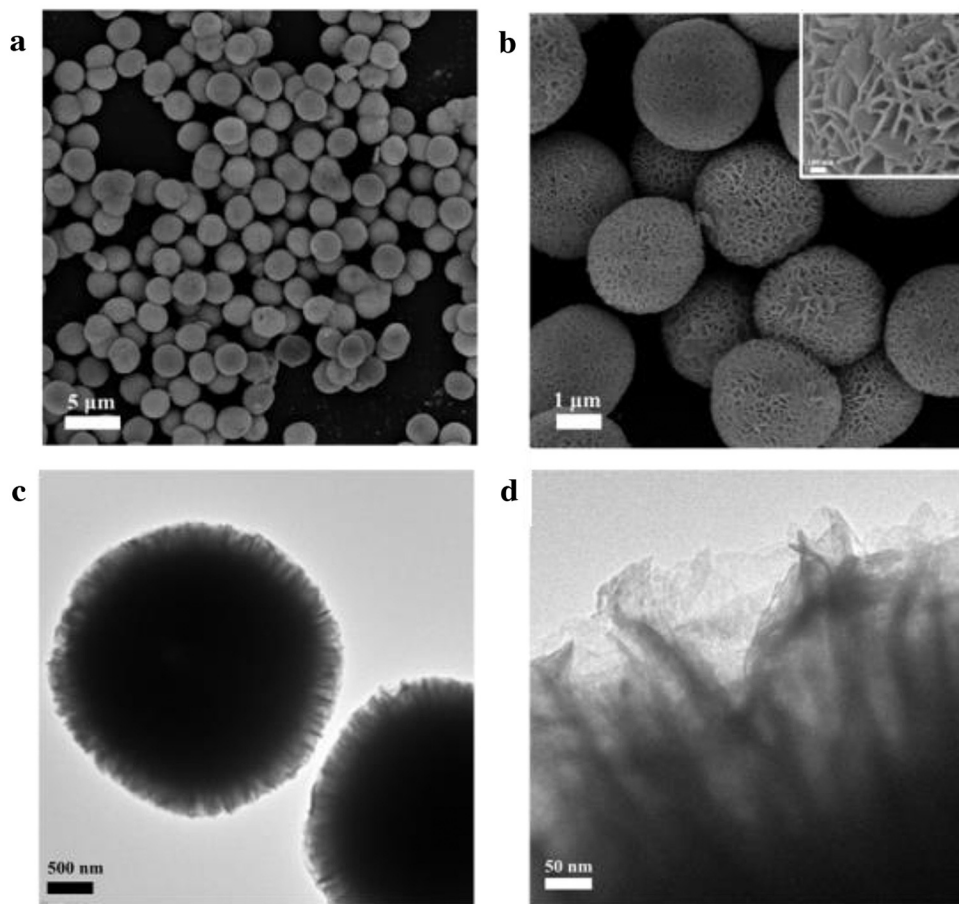


Fig. 3. SEM images (a) (b) and TEM images (c) (d) of the $\text{PbBiO}_2\text{Br}-0.10$ microspheres structures.

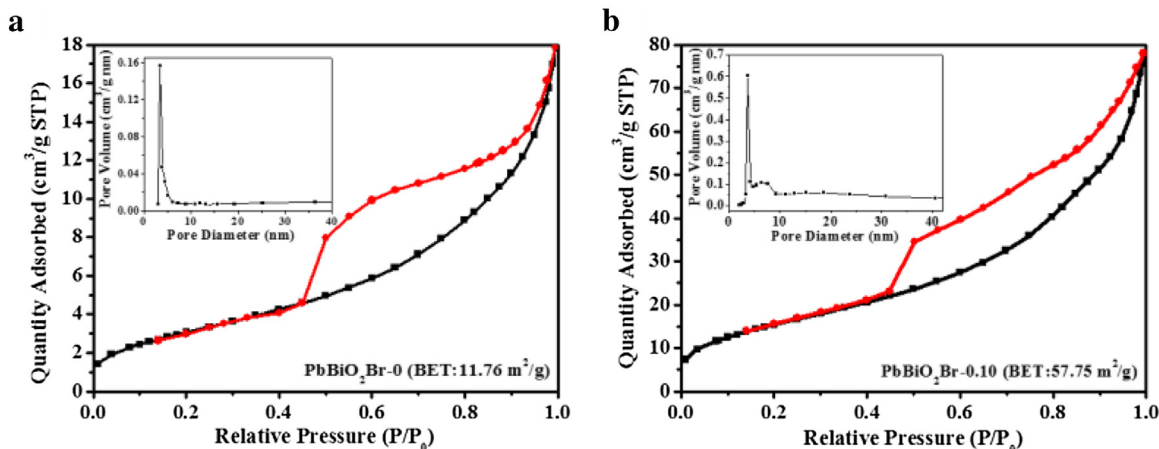


Fig. 4. Nitrogen absorption-desorption isotherms of (a) $\text{PbBiO}_2\text{Br}-0$ materials synthesized without PVP; (b) $\text{PbBiO}_2\text{Br}-0.10$ materials synthesized with 0.10 g PVP.

face area compared with other PbBiO_2Br materials of previously published literatures, which could endow better capacity of active species and reactants adsorption on the material surface [28]. In the meanwhile, a higher BET surface area could result in superior photocatalytic activity [33]. In addition, the Barrett-Joyner-Halenda (BJH) method was used to determine the pore volumes of the as-prepared PbBiO_2Br materials (inset in Fig. 4 and S3). It could be seen that the $\text{PbBiO}_2\text{Br}-0$ microsphere structures revealed mesopores of ca. 3.5 nm. Interestingly, when the PVP was introduced into the forming process of PbBiO_2Br materials, the BJH method appeared two characteristic peaks, which contained small mesopores of ca.

3.5 nm and large mesopores of from ca. 6.3 nm to 9.3 nm, and the large mesopores increased gradually with the PVP addition. The nitrogen adsorption analysis was consistent with the results of the SEM analyses.

3.2. Optical and electronics of PbBiO_2Br photocatalysts

The UV-vis diffuse reflectance spectra (DRS) of the PbBiO_2Br samples with different PVP contents are shown in Fig. S4. All of the PbBiO_2Br materials obtained by using different content of PVP had an absorption onset at 550 nm, which corresponds to a band gap

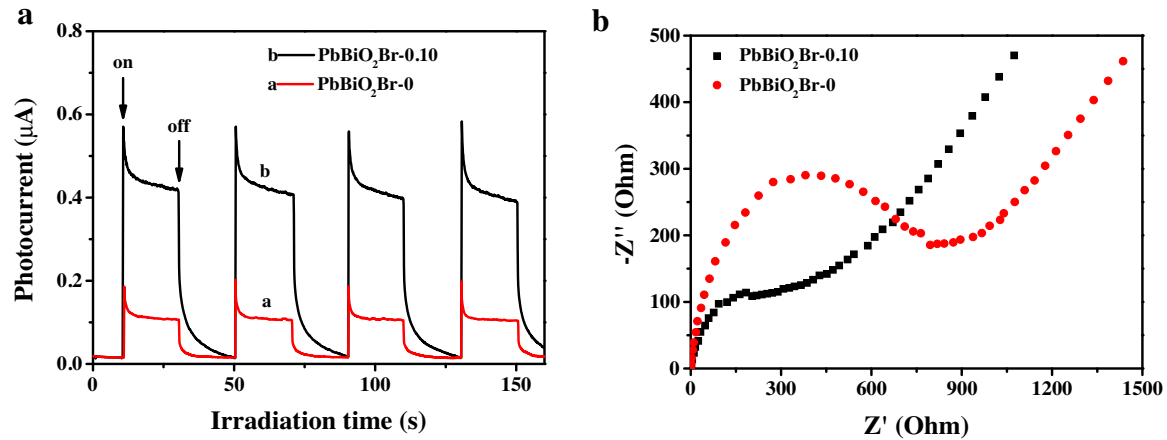


Fig. 5. (a) Transient photocurrent response and (b) electrochemical impedance spectroscopy of the as-prepared PbBiO₂Br-0 and PbBiO₂Br-0.10 materials.

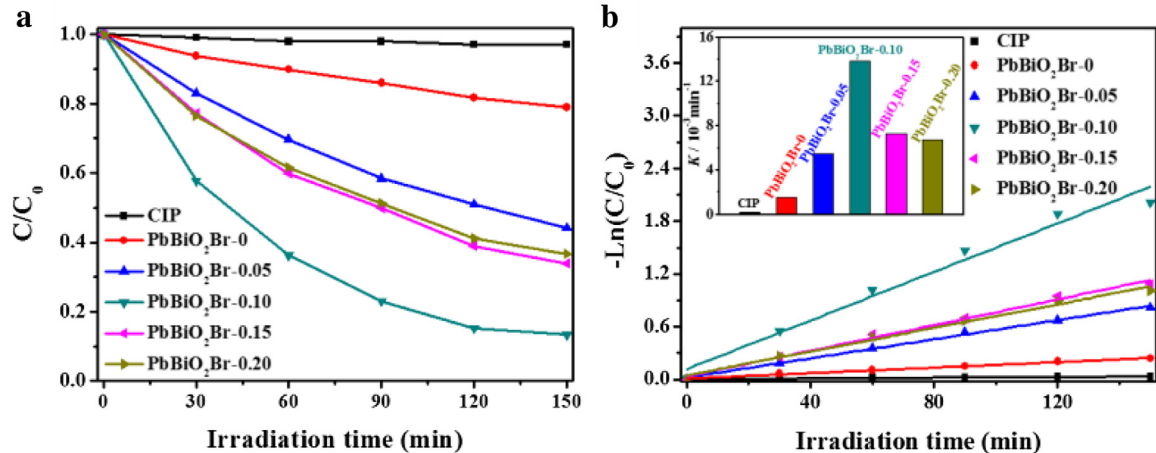


Fig. 6. (a) Photocatalytic degradation of CIP in the presence of the as-prepared PbBiO₂Br materials under visible light irradiation; (b) kinetic curves for the degradation of CIP by the as-prepared PbBiO₂Br materials.

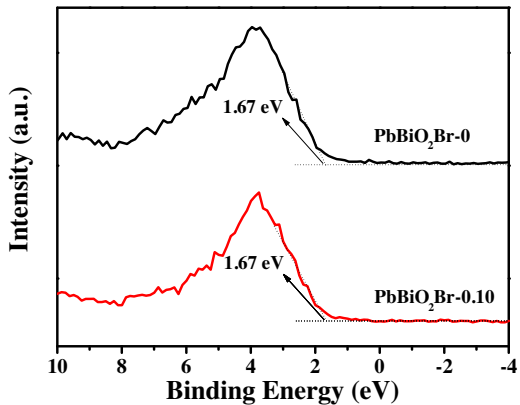


Fig. 7. XPS valence band spectra of the PbBiO₂Br-0 and PbBiO₂Br-0.10 samples.

of 2.05 eV (Fig. S4b). These results supported that the as-prepared PbBiO₂Br samples had suitable band gaps even synthesized with different PVP content. The DRS analysis indicated that the optical properties were not the main factor to influence the photocatalytic activity of the PbBiO₂Br materials [34].

To better understand the photogenerated carrier transport and charge separation performance of the as-prepared PbBiO₂Br-0 and PbBiO₂Br-0.10 materials under visible light irradiation, the

transient photocurrent responses and electrochemical impedance spectroscopy (EIS) measurements were carried out. Fig. 5a showed that the PbBiO₂Br-0.10 sample exhibited three times higher photocurrent intensity than PbBiO₂Br-0 sample. It was widely accepted that if the materials had higher the photocurrent, which would possess the higher electrons and holes separation efficiency and indicate the higher photocatalytic activity [35]. As is shown in Fig. 5b, it was found that PbBiO₂Br-0.10 had a low resistance value as compared to PbBiO₂Br-0. It is commonly recognized that the diameter of the semicircle was relative to the charge transfer resistance of the electrode surface, in which a smaller diameter corresponded to a lower resistance in the Nyquist plot [36]. The characterization results of EIS and photocurrents measurements confirmed that the addition of auxiliary PVP was a novel and effective way to improve photocatalytic efficiency.

3.3. Enhancement of photocatalytic activity

Ciprofloxacin (CIP) is the third generation quinolone antibacterial drugs, which has been used in clinical because of its wide antibiogram and excellent bactericidal effect. However, CIP abuse lead to growing resistant strains, occurring serious adverse drug reactions frequently, treating infectious disease become more difficultly, and threatening human health seriously [37]. Therefore, an effective technology is explored to remove CIP is great important and imperative. As is shown in Fig. 6, the as-prepared PbBiO₂Br

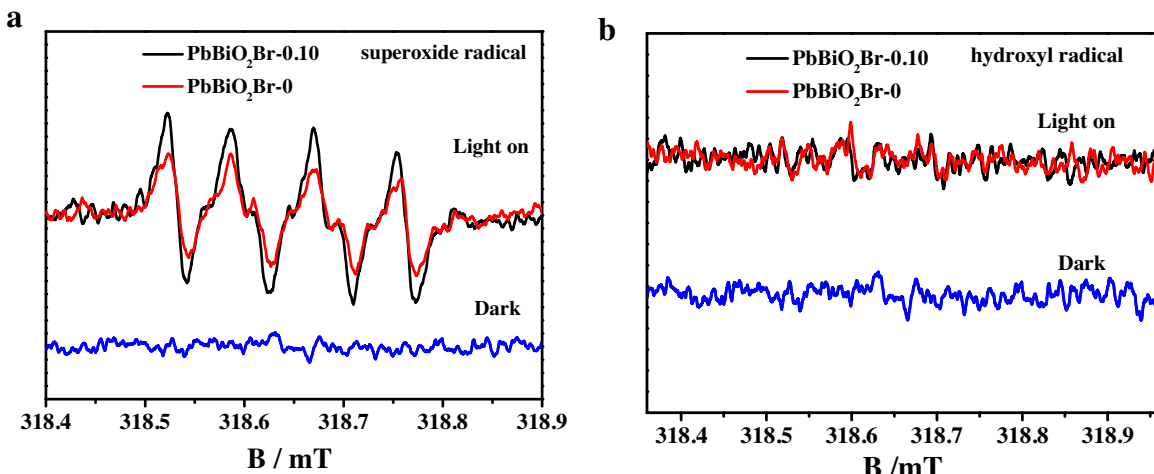


Fig. 8. DMPO spin-trapping ESR spectra recorded with the $\text{PbBiO}_2\text{Br-0}$ and $\text{PbBiO}_2\text{Br-0.10}$ samples in (a) methanol dispersion (for $\text{DMPO-O}_2^{\bullet-}$) and (b) aqueous dispersion (for $\text{DMPO-}\cdot\text{OH}$) under visible light irradiation.

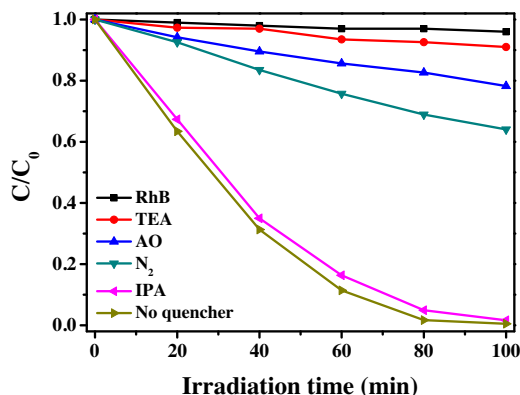


Fig. 9. Photocatalytic activities comparison of $\text{PbBiO}_2\text{Br-0.10}$ materials for the degradation of RhB with or without adding IPA, N_2 , AO, and TEA under visible light irradiation.

materials had been used for CIP degradation under visible light irradiation. Obviously, the direct photodegradation rate of CIP is extremely negligible without addition photocatalyst. After 150 min irradiation, the PbBiO_2Br microspheres obtained by using a certain amount of PVP show much higher photocatalytic activity than that of $\text{PbBiO}_2\text{Br-0}$ material. As Fig. 6a shown, the $\text{PbBiO}_2\text{Br-0.10}$ sample displayed the highest photocatalytic activity for the CIP degradation and 86.7% of CIP could be degraded after irradiation for 150 min, and the $\text{PbBiO}_2\text{Br-0}$ catalyst show poorer photocatalytic activity only 20.8% of CIP was removed. These experimental results indicated that the introduction of IL-S complex system along with microstructure change contribute to the enhanced photocatalytic performance for the photodegradation of the quinolone antibacterial drugs CIP. However, when the PVP concentration was higher than 0.10 g in IL-S complex system, a further increase of PVP content caused a decrease in the photocatalytic activity of CIP degradation. This was attributed to too many PVP lead to the microsphere structures with twisty nanosheets and even many destroyed microsphere produced, and the specific surface area decreased gradually.

Moreover, the photocatalytic degradation kinetics of CIP was investigated (Fig. 6b), which followed the pseudo-first-order reaction. It could be seen that the $\text{PbBiO}_2\text{Br-0.10}$ microspheres had the maximum rate constant of 0.01381 min^{-1} , which was 8.885 times higher than $\text{PbBiO}_2\text{Br-0}$. The relative rate constants analysis could be seen from the insert graph of Fig. 6b, which indicated different

microstructure was a significant factor on the photocatalytic activity of this system. In addition, the photocatalytic performance of $\text{PbBiO}_2\text{Br-0}$ and $\text{PbBiO}_2\text{Br-0.10}$ materials was further explored under near-infrared light. As is shown in Fig. S5, only 5% CIP could be photodegraded by $\text{PbBiO}_2\text{Br-0}$, after 5 h under near-infrared light irradiation. While photocatalytic activity of $\text{PbBiO}_2\text{Br-0.10}$ was significantly improved and nearly 47% CIP was removed. Meanwhile, the total organic carbon (TOC) removal efficiencies of CIP over $\text{PbBiO}_2\text{Br-0}$ and $\text{PbBiO}_2\text{Br-0.10}$ materials were also determined under visible light irradiation (Fig. S6). The TOC removal efficiencies of them increased gradually with the extended illumination time. After irradiation for 5 h, nearly 46.4% of CIP was mineralized by $\text{PbBiO}_2\text{Br-0.10}$ material, while only 8.3% of CIP was mineralized by $\text{PbBiO}_2\text{Br-0}$. It indicated that more CIP could be mineralized to small inorganic molecules (like CO_2 and H_2O) by $\text{PbBiO}_2\text{Br-0.10}$, which revealed that $\text{PbBiO}_2\text{Br-0.10}$ porous microspheres possessed the more outstanding photocatalytic activity than $\text{PbBiO}_2\text{Br-0}$.

In order to further explore the photocatalytic activity of the as-prepared PbBiO_2Br catalysts, a series of photocatalysis experiments selected RhB, BPA, and MB as target pollutants under visible light irradiation. As is shown in Fig. S7a, the PbBiO_2Br materials of introduction PVP soft template exhibited higher photocatalytic performance than the $\text{PbBiO}_2\text{Br-0}$ sample for the degradation of RhB. After irradiation for 100 min, only 46.7% of RhB was photodegraded by the $\text{PbBiO}_2\text{Br-0}$ materials. In the same time, the $\text{PbBiO}_2\text{Br-0.10}$ revealed the highest photocatalytic activity, about 100% of RhB was degraded. The time-dependent absorption spectra of RhB solution in the presence of $\text{PbBiO}_2\text{Br-0.10}$ microspheres is shown in Fig. S7b. Under visible light irradiation, the UV-vis absorption peak intensity of RhB decreased significantly, and the maximum absorption peak showed red shift. Meanwhile, the amaranthine RhB solution changed gradually, which became colorless after irradiation for 100 min. Meanwhile, the $\text{PbBiO}_2\text{Br-0.10}$ photocatalyst also displayed high stability, which was shown in Fig. S8, only 1.7% decrease of the photocatalytic degradation efficiency after five cycles. Moreover, the XRD analysis of $\text{PbBiO}_2\text{Br-0.10}$ material before and after the photocatalytic reactions was shown in Fig. S9, in which the crystal structures of the microspheres were not changed after five times photocatalytic cycle. These results suggested that the $\text{PbBiO}_2\text{Br-0.10}$ photocatalyst was stable during the photodegradation process.

Two different types of pollutants, such as endocrine disrupting chemical BPA [38] and biological stain MB were carried out the photocatalytic degradation by the as-prepared $\text{PbBiO}_2\text{Br-0}$ and $\text{PbBiO}_2\text{Br-0.10}$ materials, as shown in Fig. S10. All the self-

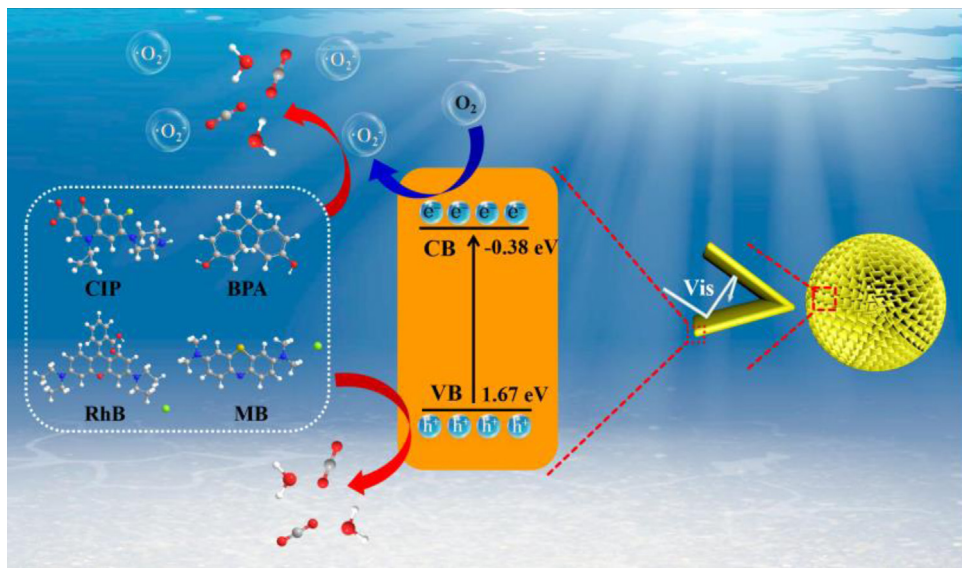


Fig. 10. Schematic of the separation and transfer for photogenerated charges in the PbBiO₂Br material combined with the possible reaction mechanism of photocatalytic procedure.

photolytic experiments of BPA and MB confirmed target pollutants photodegraded by visible light were insignificant. The results revealed that during the BPA and MB photodegradation process, the PbBiO₂Br-0.10 microspheres exhibited more superior photocatalytic activity than that of the as-prepared PbBiO₂Br-0 material. These photodegradation results of four model organic pollutant indicated that the PbBiO₂Br-0.10 material was efficient visible-light-driven photocatalyst with broad spectrum photocatalytic degradation activity. The outstanding performance of PbBiO₂Br-0.10 microspheres could become valuable photocatalyst to removal pollutants in environment.

3.4. Mechanism of pollutant photodegradation

The photocatalytic mechanism of the as-prepared PbBiO₂Br materials for the degradation of pollutants was further explored by analyzing the following experimental data. As shown in Fig. 7, the valence band (VB) potentials of PbBiO₂Br-0 and PbBiO₂Br-0.10 were determined by using XPS valence spectra [39,40]. Both PbBiO₂Br-0 and PbBiO₂Br-0.10 showed the maximum energy edge of the VB are about 1.67 eV, in which the result was similar to previously reported literature [15]. Based on the formula $E_{CB} = E_{VB} - E_g$, the CB minimum of the PbBiO₂Br materials will occur at about -0.38 eV, which implying the introduction of IL-S complex system did not affect the electronic density states of PbBiO₂Br matrix. As is known to all, the $E^0(\bullet\text{OH}/\text{OH}^-)$ is 2.38 eV vs. NHE and the $E^0(\text{O}_2/\text{O}_2\bullet^-)$ is -0.046 eV [41,42], while the VB value of PbBiO₂Br materials (1.67 eV) was less positive to oxidize OH⁻ generate •OH. However, the CB minimum of the PbBiO₂Br materials (-0.38 eV) was negative enough to reduce O₂ to yield O₂^{•-}.

The electron spin resonance (ESR) spin-trap technique was used to further confirm that the O₂^{•-} can be generated while the •OH cannot [43], when the PbBiO₂Br-0 and PbBiO₂Br-0.10 materials catalyst degrade organic pollutants during the photocatalytic reaction. As exhibited in Fig. 8a, both the PbBiO₂Br-0 and PbBiO₂Br-0.10 revealed four characteristic peaks of DMPO-O₂^{•-} under visible light irradiation, which could demonstrate the O₂^{•-} can be generated effectively during the photocatalytic process. Interestingly, the characteristic peaks of the PbBiO₂Br-0.10 were more intensive than that of PbBiO₂Br-0, which mean PbBiO₂Br-0.10 could generate further quantity of O₂^{•-} under visible light. Nevertheless, without

the DMPO-OH⁻ characteristic peaks could be found in Fig. 8b, which could be confirmed •OH was not the main reactive species in this system [44]. This result was consistent with the XPS valence band spectra analysis.

During the photocatalysis process, the active substances produced by as-prepared photocatalysts was further revealed by a series of trapping experiments, in which isopropyl alcohol (IPA) is •OH trapping agent [45], N₂ is O₂^{•-} trapping agent [46], ammonium oxalate (AO) and triethanolamine (TEA) are holes trapping agents [47,48]. As can be seen in Fig. 9, the photodegradation efficiency was not influence obviously when the IPA was added, which certified the hydroxyl radical was not the main active species, while the addition of N₂, AO and TEA greatly inhibited the degradation of RhB. Therefore, these results testified that the holes and O₂^{•-} were main active species during the photo degradation of organic contaminant process.

On the basis of photodegradation, ESR spin-trap technique and photogenerated carrier trapping test, the reaction mechanism diagram of PbBiO₂Br photocatalysts is proposed in Fig. 10. Under visible light irradiation, the as-prepared PbBiO₂Br could absorb the light more fully, due to the refraction of light took place in the porous structure. Then the photoinduced electron-hole pairs could be excited. The VB(1.67 eV) of PbBiO₂Br microspheres was less positive than $E^0(\bullet\text{OH}/\text{OH}^-)$ (2.38 eV), hence the h⁺ could not oxidize OH⁻ to yield •OH. While h⁺ could directly oxidize the organic pollutants. The CB (-0.38 eV) of PbBiO₂Br microspheres was negative than $E^0(\text{O}_2/\text{O}_2\bullet^-)$ (-0.046 eV), hence the photogenerated electrons (e⁻) on the CB of PbBiO₂Br could be trapped to produce O₂^{•-} and then participate in the photocatalytic oxidation reaction. Therefore, under visible light irradiation, the photodegradation of organic pollutants (such as: CIP, BPA, RhB, and MB) over the PbBiO₂Br microspheres surface was likely to be dominated by h⁺ and O₂^{•-} radical.

Based on the above results, several factors such as morphology, energy band structure, BET surface area, and the interfacial charge transfer rate have been addressed to explore the remarkable photocatalytic performance of the PbBiO₂Br-0.10 microspheres. Firstly, photocatalytic materials with different morphology would reveal distinct photocatalytic activity. In the SEM and TEM results, when 0.10 g PVP was added into the PbBiO₂Br catalysts, the uniform microspheres consisted of numerous PbBiO₂Br nanosheets would

be compounded. The homogeneous porous structure contribute to assist transmission of reactant and product effectively, thus promote the degradation of organic pollutants [49,50]. Secondly, the PbBiO₂Br microspheres have the narrow band-gap energy with the CB about –0.38 eV, which could reduce O₂ to generate O₂^{•-} effectually. Introduction of PVP did not change energy band structure of the as-prepared PbBiO₂Br semiconductor materials, therefore, electronic band structure was not the most important factors accelerate photocatalytic performance boost. Thirdly, the photocatalytic performance has intimate connection with the adsorption ability and surface area of the catalyst, in which the as-prepared PbBiO₂Br-0.10 with larger specific surface areas (57.75 m²/g) than other PbBiO₂Br materials could absorb more active species and reactants on its surface conduce to improving catalytic activity. Lastly, the higher photocurrent intensity and the smaller diameter of the Nyquist circle confirmed the higher interfacial charge transfer rate and enhanced photoinduced charge carrier separation efficiency of the PbBiO₂Br-0.10 microspheres. According to the above detailed analysis, it could be concluded that the enhanced photocatalytic activities of PbBiO₂Br microspheres could be a synergetic effect, including a homogeneous porous microstructure, appropriate energy band gap, higher BET surface area, faster interfacial charge transfer rate and higher separation efficiency of photogenerated electrons and holes.

4. Conclusions

In summary, novel uniform PbBiO₂Br microspheres photocatalysts have been synthesized via reactable ionic liquid [C₁₆mim]Br and appropriate PVP assisted in ethylene glycol solution. The average diameter of PbBiO₂Br microspheres was 3 μm, and the materials possessed larger specific surface area (57.75 m² g⁻¹). The PbBiO₂Br-0.10 exhibited preferable stable and higher photocatalytic activity on the degradation of organic pollutants under visible light irradiation, which could be attribute to the uniform porous microstructure, higher specific surface area, and effective interfacial charge separation. ESR spin-trap technique and photo-generated carrier trapping test indicated that O₂^{•-} and h⁺ were the main active species for the photocatalysis process. This strategy can be extended to other micro/nanostructure semiconductor materials.

Acknowledgments

This work was financially supported by the National Nature Science Foundation of China (Nos. 21476098, 21471069 and 21576123), and International Postdoctoral Exchange Fellowship Program of China Postdoctoral Council (No. 20150060). S. Dai was sponsored by the Division of Chemical Sciences, Geosciences, and Biosciences, Office of Basic Energy Sciences, U.S. Department of Energy.

Appendix A. Supplementary data

Supplementary data associated with this article can be found, in the online version, at <http://dx.doi.org/10.1016/j.apcatb.2016.12.049>.

References

- [1] H.L. Wang, L.S. Zhang, Z.G. Chen, J.Q. Hu, S.J. Li, Z.H. Wang, J.S. Liu, X.C. Wang, Chem. Soc. Rev. 43 (2014) 5234.
- [2] A. Kubacka, M. Fernández-García, G. Colón, Chem. Rev. 112 (2012) 1555.
- [3] J.R. Ran, J. Zhang, J.G. Yu, M. Jaroniec, S.Z. Qiao, Chem. Soc. Rev. 43 (2014) 7787.
- [4] W. Wang, M.O. Tadéa, Z.P. Shao, Chem. Soc. Rev. 44 (2015) 5371.
- [5] I.E. Castelli, T. Olsen, S. Datta, D.D. Landis, S. Dahl, K.S. Thygesena, K.W. Jacobsen, Energy Environ. Sci. 5 (2012) 5814.
- [6] K. Maeda, M. Eguchi, T. Oshima, Angew. Chem. Int. Ed. 48 (2014) 13164.
- [7] A. Kudo, H. Kato, S. Nakagawa, J. Phys. Chem. B 3 (2000) 571.
- [8] J.Y. Shi, G.J. Liu, N. Wang, C. Li, J. Mater. Chem. 22 (2012) 18808.
- [9] Z.L. Hua, X.Y. Zhang, X. Bai, L.L. Lv, Z.F. Ye, X. Huang, J. Colloid Interface Sci. 450 (2015) 45–53.
- [10] H.W. Huang, S.B. Wang, Y.H. Zhang, X. Han, Mater. Res. Bull. 62 (2015) 206.
- [11] X.J. Li, J. Wang, D.Y. Xu, Z. Sun, Q.S. Zhao, W.C. Peng, Y. Li, G.L. Zhang, F.B. Zhang, X.B. Fan, ACS Sustain. Chem. Eng. 3 (2015) 1017.
- [12] A. Pfitzner, P. Pohla, Angew. Chem. Int. Ed. 48 (2009) 1157.
- [13] Z.C. Shan, W.D. Wang, X.P. Lin, H.M. Ding, F.Q. Huang, J. Solid State Chem. 181 (2008) 1361.
- [14] F.Y. Xiao, J. Xing, L. Wu, Z.P. Chen, X.L. Wang, H.G. Yang, RSC Adv. 3 (2013) 10687.
- [15] M. Cherevatskaya, M. Neumann, S. Fuldner, C. Harlander, Angew. Chem. Int. Ed. 51 (2012) 4062.
- [16] R. Hayes, G.G. Warr, R. Atkin, Chem. Rev. 115 (2015) 6357.
- [17] T.L. Greaves, C.J. Drummond, Chem. Soc. Rev. 42 (2013) 1096.
- [18] J. Di, J.X. Xia, M.X. Ji, S. Yin, H.P. Li, H. Xu, Q. Zhang, H.M. Li, J. Mater. Chem. A 3 (2015) 15108.
- [19] L. Xu, J.X. Xia, L.G. Wang, J. Qian, H.M. Li, K. Wang, K.Y. Sun, M.Q. He, Chem.—A Eur. J. 20 (2014) 2244.
- [20] J.X. Xia, S. Yin, H.M. Li, H. Xu, Y.S. Yan, Q. Zhang, Langmuir 27 (2011) 1200.
- [21] J.X. Xia, H.M. Li, Z.J. Luo, K. Wang, S. Yin, Y.S. Yan, Appl. Surf. Sci. 256 (2010) 1871.
- [22] Z.H. Li, Z.M. Liu, J.L. Zhang, B.X. Han, J.M. Du, Y.A. Gao, T. Jiang, J. Phys. Chem. B 109 (2005) 14445.
- [23] M.P. Singha, R.K. Singh, S. Chandra, Prog. Mater. Sci. 64 (2014) 73.
- [24] F. Gao, J. Hu, C.J. Peng, H.L. Liu, Y. Hu, Langmuir 28 (2012) 2950.
- [25] H. Kaper, I. Djerdj, S. Gross, H. Amenitsch, M. Antonietta, B.M. Smarsly, Phys. Chem. Chem. Phys. 17 (2015) 18138.
- [26] T.T. Li, S.L. Luo, L.X. Yang, Mater. Lett. 109 (2013) 247.
- [27] J.X. Xia, J. Zhang, S. Yin, H.M. Li, H. Xu, L. Xu, Q. Zhang, J. Phys. Chem. Solids 74 (2013) 298.
- [28] J.X. Xia, S. Yin, H.M. Li, H. Xu, L. Xu, Y.G. Xu, Dalton Trans. 40 (2011) 5249.
- [29] C.M. Xiong, W. Wang, F.T. Tan, F. Luo, J.G. Chen, X.L. Qiao, J. Hazard. Mater. 299 (2015) 664.
- [30] J. Di, J.X. Xia, S. Yin, H. Xu, L. Xu, Y.G. Xu, M.Q. He, H.M. Li, J. Mater. Chem. A 2 (2014) 5340.
- [31] Y.T. Jing, H.W. Wang, J. Zhao, H. Yi, X.F. Wang, Appl. Surf. Sci. 347 (2015) 499.
- [32] J.G. Yu, J.X. Low, W. Xiao, P. Zhou, M. Jaroniec, J. Am. Chem. Soc. 136 (2014) 8839.
- [33] M.Y. Hsu, H.L. Hsu, J. Leu, J. Electrochem. Soc. 159 (2012) 722.
- [34] X.H. Gao, H.B. Wu, L.X. Zheng, Y.J. Zhong, Y. Hu, X.W. Lou, Angew. Chem. Int. Ed. 53 (2014) 5917.
- [35] J. Di, J.X. Xia, S. Yin, H. Xu, M.Q. He, H.M. Li, L. Xu, Y.P. Jiang, RSC Adv. 3 (2013) 19624.
- [36] L. Zhang, H.B. Wu, Y. Yan, X. Wang, X.W. Lou, Energy Environ. Sci. 7 (2014) 3302.
- [37] T. Paul, P.L. Miller, T.J. Strathmann, Environ. Sci. Technol. 41 (2007) 4720.
- [38] S.C. DCruz, R. Jubendradass, P.P. Mathur, Reprod. Sci. 19 (2012) 163.
- [39] J.C. Woicik, E.J. Nelson, L. Kronik, M. Jain, J.R. Chelikowsky, D. Heskett, L.E. Berman, G.S. Herman, Phys. Rev. Lett. 89 (2002) 077401.
- [40] X.B. Chen, L. Liu, P.Y. Yu, S.S. Mao, Science 331 (2011) 746.
- [41] L.Q. Ye, J.N. Chen, L.H. Tian, J.Y. Liu, T.Y. Peng, K.J. Deng, L. Zan, Appl. Catal. B: Environ. 130–131 (2013) 1.
- [42] H.F. Cheng, B.B. Huang, Y. Dai, X.Y. Qin, X.Y. Zhang, Langmuir 26 (2010) 6618.
- [43] C.C. Han, L.E. Wu, L. Ge, Y.J. Li, Z. Zhao, Carbon 92 (2015) 31.
- [44] Y.H. Lv, Y.Y. Zhu, Y.F. Zhu, J. Phys. Chem. C 117 (2013) 18520.
- [45] J. Di, J.X. Xia, Y.P. Ge, L. Xu, H. Xu, M.Q. He, Q. Zhang, H.M. Li, J. Mater. Chem. A 2 (2014) 15864.
- [46] S.Q. Huang, Y.G. Xu, Z.G. Chen, M. Xie, H. Xu, M.Q. He, H.M. Li, Q. Zhang, RSC Adv. 5 (2015) 71035.
- [47] J. Cao, B.Y. Xu, H.L. Lin, B.D. Luo, S.F. Chen, Chem. Eng. J. 185–186 (2012) 91.
- [48] S.Q. Huang, Y.G. Xu, M. Xie, H. Xu, M.Q. He, J.X. Xia, L.Y. Huang, H.M. Li, Colloids Surf. A: Physicochem. Eng. Asp. 478 (2015) 71.
- [49] J.G. Yu, L.J. Zhang, B. Cheng, Y.R. Su, J. Phys. Chem. C 111 (2007) 10582.
- [50] Q. Sun, X.R. Jia, X.F. Wang, H.G. Yu, J.G. Yu, Dalton Trans. 44 (2015) 14532.